Irrigation Science
https://doi.org/10.1007/s00271-021-00752-0

ORIGINAL PAPER

Time-series clustering of remote sensing retrievals for defining management zones in a vineyard

Noa Ohana-Levi[1,2] · Feng Gao[3] · Kyle Knipper[3] · William P. Kustas[3] · Martha C. Anderson[3] · Maria del Mar Alsina[4] · Luis A. Sanchez[4] · Arnon Karnieli[1]

Received: 13 June 2021 / Accepted: 5 October 2021

Abstract

Management zones (MZs) are efficient for applying site-specific management in agricultural fields. This study proposes an approach for generating MZs using time-series clustering (TSC) to also enable time-specific management. TSC was applied to daily remote sensing retrievals in a California vineyard during four growing seasons (2015–2018) using three datasets: evapotranspiration (ET), leaf area index (LAI), and normalized difference vegetation index (NDVI). Distinct MZs were delineated based on similarities in pixel-level temporal dynamics for each dataset, using dissimilarity index to determine the optimal number of clusters and compare TSC results. The differences between the cluster centers were calculated, along with the ratio between the centers' differences and the range of each dataset, denoting the degree of difference between MZs centers. Similarity between MZs from each factor was quantified using Cramer's V and Fréchet distances. Finally, an aggregated (multi-factor) MZ map was generated using multivariate clustering. The resulting MZs were compared to a 2016 yield map to determine the significance of differences between means and distribution among MZs. The findings show that LAI TSC achieved the best cluster separation. The NDVI and LAI MZs maps were nearly identical (Cramer's V of 0.97), while ET showed weaker similarities to NDVI and LAI (0.61 and 0.62, respectively). Similar findings were observed for the Fréchet distances. The yield values were found to be significantly different among MZs for all TSC maps. TSC may be further utilized for defining within-field spatial variability and temporal dynamics for precision irrigation practices that account for spatial and temporal variability.

Introduction

The information revolution in the agricultural sector presents new opportunities for characterizing attributes in the field, quantifying their spatial variability, and analyzing their causes (Coble et al. 2018). Precision agriculture (PA) is a management strategy that takes into account various datasets collected in the field to support decisions and actions to increase efficiency, productivity, and sustainability of agricultural processes (Pathak et al. 2019). A common

✉ Noa Ohana-Levi
noao@post.bgu.ac.il

Feng Gao
feng.gao@usda.gov

Kyle Knipper
kyle.knipper@usda.gov

William P. Kustas
bill.kustas@usda.gov

Martha C. Anderson
martha.anderson@usda.gov

Maria del Mar Alsina
mariadelmar.alsina@ejgallo.com

Luis A. Sanchez
Luis.Sanchez@ejgallo.com

Arnon Karnieli
karnieli@bgu.ac.il

[1] The Remote Sensing Laboratory, Swiss Institute for Dryland Environmental and Energy Research, Jacob Blaustein Institutes for Desert Research, Ben-Gurion University of the Negev, Sede Boker, 84990 Beersheba, Israel

[2] Variability, 85512 Ashalim, Israel

[3] Hydrology and Remote Sensing Laboratory, USDA ARS, Beltsville, MD 20705-2350, USA

[4] E.&J. Gallo Winery, Vit, iculture, Chemistry and Enology, Modesto, CA 95354, USA

Published online: 18 October 2021

management technique for applying PA is based on partitioning agricultural fields into homogeneous sub-units, termed management zones (MZs). MZs are defined according to spatially varying properties in the field (Córdoba et al. 2016; Ohana-Levi et al. 2021) and enable various site-specific management (SSM) applications, such as irrigation (Haghverdi et al. 2015; Ohana-Levi et al. 2019a), fertilization (Nawar et al. 2017; Peralta et al. 2015), and pest-control (Park et al. 2007). The minimum size of MZs is proportional to the ability of the grower to differentially manage sub-units within the field (Albornoz et al. 2018; Zhang et al. 2002).

The datasets most used for MZ delineation include spatially varying static attributes such as terrain, soil, and plant characteristics from one or more data layers. The resulting MZs are expected to be simple, stable over the years, and feasible for differential management practices (Nawar et al. 2017). In recent years, however, there has been an increasing focus on temporally varying MZs, suggesting that different timeframes within the growing season are characterized by dynamic spatial patterns throughout the field (Knipper et al. 2019a,b; McBratney et al. 2005). O'Shaughnessy et al. (2015) successfully implemented a plant feedback system that relies on a wireless sensor network of infrared thermometers (IRTs). They used this system to develop dynamic prescription maps to accomplish adaptive irrigation scheduling for cotton in a center-pivot field during two growing seasons. Fontanet et al. (2020) used time series of remotely sensed vegetation index along with soil moisture sensor measurements and root zone simulation forecasts to generate dynamic MZs designed for variable rate irrigation scheduling throughout the growing season in a maize field. These studies promote dynamic management in the field and do not consider the spatial characteristics of the whole-seasonal temporal variation. However, the dynamic properties within the field, which are becoming commonly available at high temporal scales (less than a week) via satellite imagery, may be used to generate static MZs (Ohana-Levi et al. 2020a,b,c,d). This approach provides information on both the temporal and spatial characteristics in a field, which may be utilized for SSM applications as well as time-specific management (TSM).

Temporal datasets generated through remotely sensed imagery are suited for quantifying plant conditions within the field through space and time. Some satellite-derived datasets may be easily acquired at high temporal and spatial resolutions, providing a suitable platform for time-series analysis. Earth observation retrievals are commonly used for representing different aspects of grapevine conditions at the vineyard scale, such as evapotranspiration (ET; Knipper et al. 2019b), leaf area index (LAI; White et al. 2018), and normalized difference vegetation index (NDVI; Sun et al. 2017). All three variables are widely used in agricultural practices and enable partitioning of the field into different groups suitable for SSM. Specifically in vineyards, these variables are related to yield spatial variability (Arab et al. 2021; Noa Ohana-Levi et al. 2019a) and distribution across the field, which may assist in optimization of yield amounts through smart management of the field. ET is the process in which water stored in the soil or vegetation is transferred to the atmosphere as vapor through plant transpiration and direct evaporation (Maes and Steppe 2012). ET is an essential measure for determining water stress and water conditions of crops for irrigation purposes and has been successfully quantified using thermal imagery for agricultural practices in vineyards at the field scale (Knipper et al. 2019a,b; Semmens et al. 2016; Xia et al. 2016). ET was found to be provide valuable information for yield estimation (Sun et al. 2017) and an understanding of the relations between vineyard water stress and yield (Knipper et al. 2019a). LAI is the ratio of the area of foliage to the ground surface area with respect to the direction of radiation (Monteith and Unsworth 2013; Watson 1947) and, at vineyard level, it is used to assess the spatial variability of canopy growth and density within the field, and has been used to estimate grapevine health in vineyards (Mathews and Jensen 2013), pruning weight (Johnson et al. 2003), and grape yield (Sun et al. 2017). NDVI is derived using the red and near-infrared spectral bands and is associated with the levels of photosynthetically active radiation absorbed by the canopy (Tucker 1979). NDVI has been widely applied in studies performed over vineyards and was shown to be spatially associated with the grapevine development through time (Kazmierski et al. 2011), water stress (Acevedo-Opazo et al. 2008; Ohana-Levi et al. 2019a), yield (Cunha et al. 2010; Sun et al. 2017), bud differentiation (Cunha et al. 2010), and additional characteristics in the vineyard.

LAI and NDVI have been shown to be strongly related in vineyards (Johnson et al. 2003) and reflect similar spatial and temporal patterns (Hall et al. 2008; Sun et al. 2017). ET was found to be affected by LAI throughout the growing season (Netzer et al. 2009; Ohana-Levi et al. 2020a,b,c,d; Vanino et al. 2015). Strong relations were also determined between NDVI and ET-related measures, such as the crop coefficient (Campos et al. 2010; Er-Raki et al. 2013). In many studies, soil properties such as water content and type were found to indirectly affect ET (Azevedo et al. 2008; Ohana-Levi et al. 2020a), LAI (Azevedo et al. 2008), and NDVI (Martínez-Casasnovas et al. 2010). Therefore, the spatial variability of these measures might be expected to be somewhat similar throughout the vineyard.

Multitemporal datasets composed of multiple images provide sets of time series. The latent spatial variability of the image time series can be extracted for a specific area during a specific timeframe. This process can be performed using various approaches for analyzing the temporal dynamics for each pixel in the image. Recent studies used multiple images

to extract the long-term trend of each pixel, using methods such as Mann-Kendell test for monotonic trend (Kumar et al. 2017; Ohana-Levi et al. 2019b), the Cox-Stuart test (Militino et al. 2020), or the modified Seasonal Kendall test for cyclic datasets (de Jong et al. 2011). Alternatively, time-series vectors, one for each pixel, may be compared throughout the spatial domain by clustering the pixels into homogeneous groups according to the similarities of their temporal dynamics (Aghabozorgi et al. 2015). This time-series clustering (TSC) strategy is commonly applied with remote sensing data for land-cover mapping (Gómez et al. 2016; Petitjean et al. 2012; Zhang et al. 2017, 2014). TSC has also been applied for other cases; for example, Liu et al. (2018) applied three techniques of TSC to land surface temperature (LST) time-series products derived from MODerate-resolution Imaging Spectroradiometer (MODIS) satellite images. Xu et al. (2018) used k-means over a time series of Synthetic Aperture Radar (SAR) imagery derived from Sentinel 1 to generate temporal models of crops to classify crop categories in Wuqing District, Tianjin city, China. Several studies used time series of NDVI images to apply TSC (Romani et al. 2011; Viovy 2000). However, TSC has rarely been used to quantify spatial variability in agricultural fields (Ohana-Levi et al. 2020a; Romani et al. 2011).

This research is part of the Grape Remote-Sensing Atmospheric Profile and Evapotranspiration eXperiment (GRAPEX) (Kustas et al. 2018) conducted by the Agricultural Research Service of the United States Department of Agriculture (USDA—ARS) and E&J Gallo Winery. The goal is to apply TSC over several datasets of daily time series of images to generate MZs at the field scale, which has been rarely achieved, to the best of our knowledge. Ohana-Levi et al. (2020a,b,c,d) applied TSC to partition a vineyard into MZs using different time components based on remote sensing retrievals of ET and relating the resulting MZs to environmental characteristics in the field including soil type, lithology, elevation, slope, aspect, and topographic wetness index. This current study extends the use of TSC based on remotely sensed imagery to other earth observation retrievals such as LAI and NDVI, which are accessible in high spatial and temporal resolutions.

In recent years, there has been a growing focus on SSM in agricultural fields using various techniques such as MZs, mostly relying on the spatial variation of soil and crops (Khosla et al. 2010). In this present work, we propose a framework to enable defining MZs using time series based on satellite retrievals of crop characteristics, in this case, ET, LAI, and NDVI. This way, the resulting MZs not only provide the spatial pattern within the field but also display the temporal dynamics typical of each MZ, as well as the underlying temporal differences between the MZs. This allows us to understand the extent of variation in crop conditions through time in the field, within each MZ, and between MZs, and may be used for better assessment of typical plant conditions during the various phenological growth stages. The suggested framework may assist in SSM and TSM based on the monitoring of plant conditions throughout multiple seasons. The overarching goal was to generate field MZs using different sets of time-series data based on remote sensing imagery. The specific objectives included: (1) generating MZs using TSC based on ET, LAI and NDVI time-series at a daily scale; (2) comparing the TSC performance among the three sets of time series; (3) defining MZs in the vineyard using multivariate clustering of the ET, LAI, and NDVI time series; and (4) relating the distributions of the MZs of each dataset with spatial variability in grape yield. Defining the relationships between the MZs and grape yield may assist in developing strategies for optimizing yield based on vegetative and water constraints.

Methodology

Study area

The study was conducted in a 'Pinot noir' vineyard located near Lodi, in the Central Valley of California (Fig. 1), characterized by a Mediterranean climate. This is a 35 ha drip irrigated vineyard planted in 2009. The vines are trained in a split canopy, and the row orientation is east–west, with a spacing of 1.5 m between vines and 3.3 m between rows. The phenological cycle of the vineyard typically includes budbreak in mid-late March and harvest in late August. The vineyard area contains locations that were not planted with vines, including two vernal pools and a vineyard management complex. These locations were masked out of the research area. Additionally, pixels at the vineyard borders were removed to avoid mixed-pixel effects and the impact of border vines that are influenced by external sources (Murolo et al. 2014).

Data collection—ET, LAI, and NDVI images

Three time-series datasets were generated based on satellite imagery, combining data from multiple sensors using data fusion. Each dataset included images of specific measures, namely ET, LAI, and NDVI. All three time series were collected during four consecutive growing seasons during 2015–2018. Each growing season was defined between March 1 until October 31, with a total of 245 days per season (example of such time series for a specific pixel is illustrated in Fig. 2) to capture the full growth cycle of the grapevines and photosynthetic activity, accumulating to a total of 980 images for each dataset. The three time-series datasets are further described.

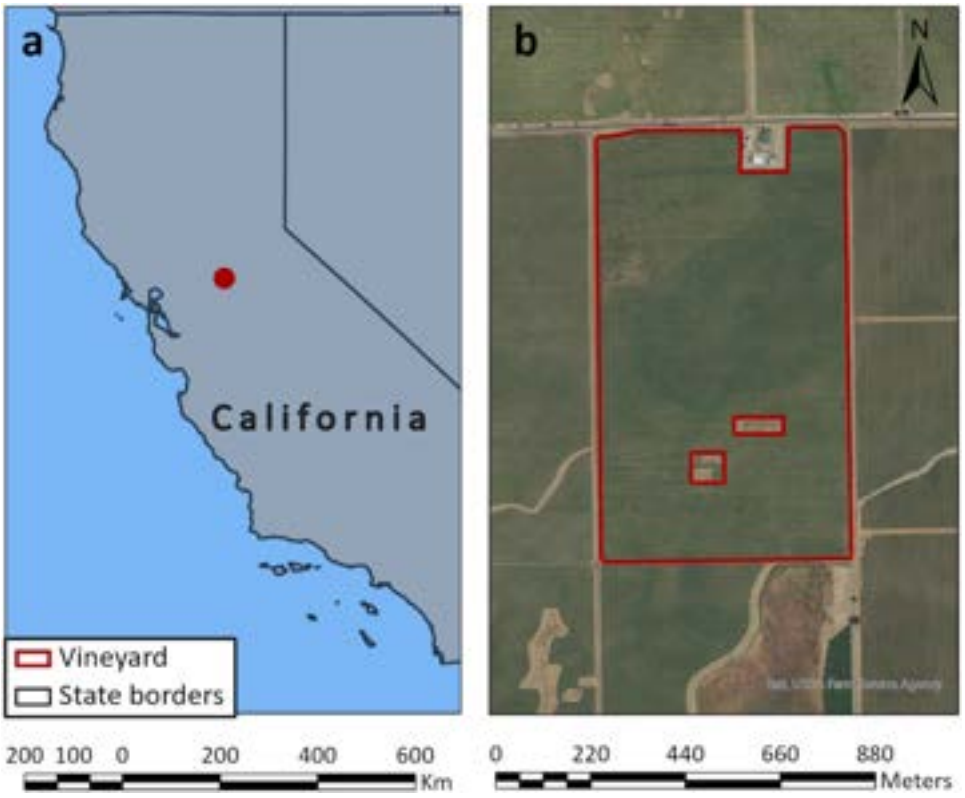

Fig. 1 The research area located in the Central Valley of California (**a**), consisting of a *Vitis Vinifera* Pinot noir vineyard (**b**)

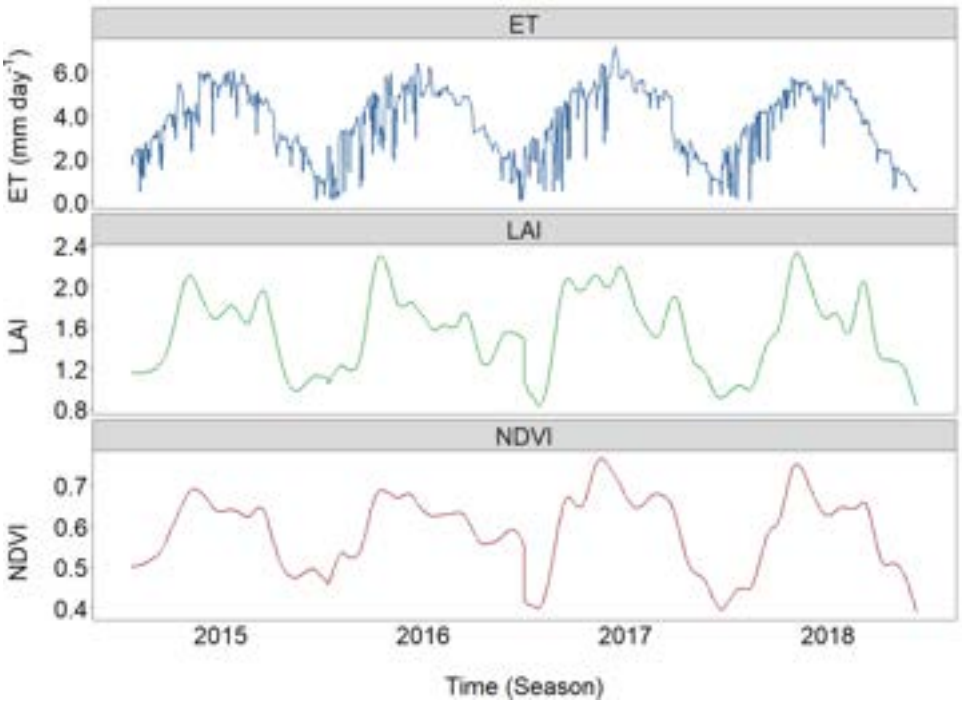

Fig. 2 Visualization of the multiseasonal time series of evapotranspiration (ET), leaf area index (LAI), and normalized vegetation difference index (NDVI) for a specific pixel. Each season begins on March 1 and ends on October 31. The values during the winter were eliminated from the datasets

ET image series

In this study, the Atmosphere-Land Exchange Inverse (ALEXI) model (Anderson et al. 2007) and the associated flux disaggregation technique (DisALEXI) (Norman et al. 2003) were used along with the Spatial and Temporal Adaptive Reflectance Fusion Model (STARFM) (Gao et al. 2006) to blend ET timeseries from Landsat and MODIS. ALEXI

relates the temporal dynamics of morning LST, derived from geostationary satellites, to atmospheric boundary growth affected by surface moisture availability and heat flux to estimate daily 4 km ET fluxes. These images are too coarse for field-scale applications and were, therefore, spatially downscaled (DisALEXI) using higher resolution LST data based on thermal infrared (TIR) imagery from MODIS (1 km) and Landsat (30 m). STARFM was then used to combine Landsat and MODIS ET images and produce daily 30 m ET maps. Detailed descriptions of the ET modeling process may be found in Cammalleri et al. (2014) and Anderson et al. (2018). Previous studies presented good agreement between ET derived by ALEXI/DisALEXI and measurements from eddy covariance flux tower (Knipper et al. 2020; Knipper et al. 2019a,b; Semmens et al. 2016). Applications over the current vineyard near Lodi were presented by Semmens et al. (2016), and Knipper et al. (2019a,b, 2020).

LAI image series

Daily 30 m LAI time series from 2015 to 2018 were generated using the Harmonized Landsat and Sentinel-2 (HLS) surface reflectance (SR) (Claverie et al. 2018) through two steps. In the first step, LAI images at HLS acquisition dates were produced using regression trees trained from the high-quality MODIS LAI retrievals and field LAI measurements. The reference-based regression tree approach was developed to make a MODIS-consistent LAI product at 30 m resolution (Gao et al. 2012) and has been assessed over California vineyards using Landsat imagery (Sun et al. 2017). In the current project, homogeneous and high-quality LAI retrievals from MODIS LAI products (MCD15A3H, 4 day, 500 m) were extracted from 2014 to 2019. The corresponding HLS surface reflectance values for the sampled MODIS pixels were averaged to 500 m resolution to create 500 m LAI-SR records. LAI field measurements ($n = 260$) from three GRAPEX sites [Sierra Loma (Lodi), Ripperdan, and Barrelli] (White et al. 2018) from 2013 to 2019 were paired with 30 m HLS SRs extracted from the measurement locations to generate 30 m LAI-SR records. Two types of LAI-SR records were combined using the weighting strategy similar to Gao et al. (2014). The regression trees were then built using the combined 500 m and 30 m records. The trained regression trees were applied to the HLS SR to generate 30 m LAI maps on Landsat or Sentinel-2 acquisition dates. In the second step, a local moving Savitzky–Golay (SG) filter was used to remove noise, smooth data, and fill temporal gaps (Gao et al. 2020). Noisy data points outside three standard deviations of the mean error were removed. For each pixel, the 2nd order polynomial fitting function was built from noise-free observations within the local moving window to fill gaps and smooth LAI to generate daily 30 m LAI time series.

NDVI image series

The 30-m NDVI images at Landsat or Sentinel-2 acquisition dates were produced using HLS SR from red and NIR bands. Cloud pixels identified in the HLS quality assurance (QA) layer were excluded. Daily 30 m NDVI time series from 2015 to 2018 were generated using the same local moving SG filter approach as for LAI.

Yield map

The resulting MZ patterns were visually and quantitatively compared with spatial patterns grape yield across the study vineyard. Yield was mapped during harvest on August 22, 2016 by E&J Gallo Winery using an Advanced Technology Viticulture (ATV, Joslin, Australia) yield monitoring system. A conversion of mass flow units into tons per hectare was conducted, eliminating outliers (yield data greater than three standard deviations from the mean), and normalized across harvesters. The yield map was interpolated to a 3 m grid using Vesper Spatial Prediction Software for Precision Agriculture (Whelan et al. 2002). Yield maps for other growing seasons were not included due to unreliable or missing data.

Time-series clustering

A time series is defined as a set of observations recorded at specific time intervals (Brockwell and Davis 2016), while observations of time series are recorded continuously. TSC partitions multiple time series into homogenous groups depending on the similarities between each pair of time series within the dataset (Aghabozorgi et al. 2015). The datasets were prepared and analyzed as described below.

Data preparation

First, non-production areas (vernal pools, vineyard management complex, and border pixels) were removed from each dataset, as described in Sect. "Study area". For each dataset, outliers were in pixel-level time series were identified using the interquartile range (IQR) technique. A value was considered an outlier if it was higher than the sum of the third quantile and two times the IQR, or lower than the difference between the first quantile and two times the IQR. Values over/under the averaged high/low outliers were removed from the dataset. Further, missing values were interpolated by a moving average technique, using the "imputeTS" package in R (Moritz and Bartz-Beielstein 2017) a window of 4 days. Finally, since the cycles of each time-series dataset were relatively similar, a dimensionality reduction approach was taken (Aghabozorgi et al. 2015). Each of the datasets included values corresponding to identical dates during each growing season. The time series for each pixel in each

dataset (ET, LAI, and NDVI) were aggregated to produce a mean seasonal profile representation. The aggregation computation creates one seasonal profile, representing the typical seasonal values for each pixel in the vineyard. The length of representation is the length of the time-series frequency (e.g., the number of days defined for each growing season), including 245 (March 1–October 31) mean daily values. The seasonal representation was computed using "TSrepr" package in R (Laurinec 2018).

Fuzzy c-means clustering

A clustering algorithm was then applied to the image time series. First, a pair-wise distance matrix of each time series was computed. A distance matrix may be generated using various techniques of distance measures that consider the dynamic changes in time series, such as dynamic time-warping, Hausdorff distance, Longest Common Sub-Sequence, and many more (Aghabozorgi et al. 2015). However, since in our case the similarities among pixels with the actual values of ET, LAI, and NDVI per day are of interest, we used the Euclidean distance measure to produce the distance matrix (Aghabozorgi and Wah 2014). The fuzzy c-means (FCM) clustering algorithm was used to apply the TSC. A fuzzy set includes fuzzy boundaries where each observation is assigned a degree of membership to each set. FCM partitions a collection of observations into c fuzzy groups. The algorithm detects a cluster center in each group, such that the dissimilarity measure between the center and the values of the different observations within the cluster is minimized (Gath and Geva 1989). The FCM algorithm was applied to each time-series dataset with $2 \leq c \leq 6$. The number of groups used to define the MZs was assigned based on the TSC with the best separation among clusters and the highest similarities within the clusters, with a maximum of $c = 6$ assumed as a practical limit for vineyard management. The clustering was performed using the R package "ppclust" (Cebeci et al. 2019). The resulting partitioning was evaluated using the silhouette index. This index measures the degree of similarity between each observation and its cluster center compared to other cluster centers (Rousseeuw 1987). The silhouette width ranges from − 1 and 1, with higher values indicating better similarity to the assigned cluster. The average silhouette width (ASW) was computed using the "cluster" R package (Maechler et al. 2019).

For each time-series dataset, a TSC map was generated (shown in sub-section Time-series clustering), and each TSC map was linked to complementary time-series plots. These plots show the time series of the centers of each cluster, along with the time series of the various pixels assigned to each cluster. An additional plot was produced to show the difference among the cluster centers (Ohana-Levi et al. 2020a) (the plots are available in sub-section Time-series clustering). Furthermore, a ratio denoting the magnitude of difference between cluster centers was computed as the difference range among cluster centers was divided by the range of the dataset values. In other words, values of the difference range for each dataset was normalized to the data range to indicate the strength of the difference between MZs, with a higher ratio value signifying a larger difference.

Finally, the TSC assessment for each time-series dataset was performed using the ASW measure. For each TSC map, two ASW values were calculated: ASW of each cluster, and a global ASW value, averaging the ASW values of the different clusters.

Comparison among ET, LAI, and NDVI time-series clustering

Dissimilarity measures were calculated to quantitatively assess the differences between TSC results from the three different datasets. A Cramer's V statistic was computed for each pair of TSC maps. Cramer's V is a statistical test designed to estimate the strength of an association between two categorical variables and ranges between 0 and 1 (Akoglu 2018). Therefore, values closer to 1 denote higher similarities between paired TSC.

Additionally, the centroid values of the different clusters and the values of the difference among the cluster centers were normalized using the empirical cumulative distribution function. These normalized vectors were then compared using the Fréchet distance, which considers the location and ordering of the points along the curves and enables measuring the similarity between two curves (Alt and Godau 1995). The Fréchet distance between two curves describes the minimum length between them. Values approaching zero, signify strong similarities among curves. The higher the resulting value, the longer the distance between the curves, and they are considered dissimilar. This analysis was used for assessing the resemblance between the curves of the different cluster centers and their differences for each pair of datasets.

Multivariate time-series clustering

The process of TSC described in sub-section Time-series clustering time-series clustering resulted in three TSC maps: for ET, LAI, and NDVI. After comparing the TSC performance and the spatial and temporal patterns of these three maps, they were aggregated into one final MZ map for the vineyard. In the case where a pair of TSC showed strong association via the Cramer's V test, one of the maps was removed from the multivariate clustering procedure. The multivariate clustering was performed by calculating the distance matrix of the categorical variables, where all TSC maps have c categories. The Gower's similarity coefficient (Gower 1971) was used to generate the distance matrix, which was then used to run a partition around medoids

(PAM) clustering algorithm (Kaufman and Rousseeuw 1990) and generate an aggregated MZ map. The PAM algorithm searches for c representative objects, or medoids, among the observations in the dataset. After locating c medoids, each observation is assigned to its nearest medoid. An iterative process is applied to minimize the dissimilarities of the observations to their closest medoid (Reynolds et al. 2006). The bivariate clustering procedure was applied using the R package "cluster" (Maechler et al. 2019).

Comparison of management zones using the yield map

To assess whether the MZs, delineated using the time series of each dataset (ET, LAI, NDVI) and the multivariate clustering, are compatible with yield spatial variability, two statistical analyses were conducted. These analyses used the continuous values of the 2016 yield map (described in sub-section Yield map) and the clusters of each dataset as categorical variables. First, an unpaired t test was applied to the pairs of clusters for each dataset to assess the differences between means (Ohana-Levi et al. 2020a). Second, a Kolmogorov–Smirnov test (Lilliefors 1967) between all paired cluster centers was used to assess the similarity between distributions (Noy et al. 2021). These statistical tests were conducted using R (R Core Team 2020).

Results

Time-series clustering

The original time-series datasets of ET, LAI, and NDVI were composed of 980 images that were aggregated to allow seasonal representation for each dataset. The aggregated time-series datasets were used to partition the vineyard into MZs according to similarities in pixel-level temporal dynamics. The optimal number of clusters was selected using the ASW index for $2 \leq c \leq 6$, while two clusters achieved the highest score (Table 1), and each dataset was clustered accordingly. Figure 3 illustrates the TSC maps delineating the MZs, while Table 2 provides the supporting statistics for the TSC maps giving the ASW dissimilarity measure for both clusters and for the entire vineyard. LAI received the highest ASW score, tightly followed by NDVI (0.49 and 0.47, respectively), signifying a better separability between the clusters than for the ET TSC map. Cluster 2 was characterized by weaker similarities to the cluster centers than Cluster 1 for all three TSC maps.

For each TSC map, three plots were generated showing the temporal dynamics of each cluster center and the difference between the centers of clusters 1 and 2 (Fig. 4). The general temporal pattern was similar among all datasets. Cluster 2 had lower values than Cluster 1 for all datasets, while both showed a sharp increase during the early season, followed by stabilization during June and July, and a decrease towards the end of the growing season. For all datasets, the differences between the cluster centers (Fig. 4a-c, bottom panels) showed the highest similarities at the beginning of the season. While the season progressed, the differences between the time series of the two clusters increased. The strongest difference between clusters was attributed to LAI (Table 3), with a 40% difference range to the data range ratio. The strongest similarities between clusters were

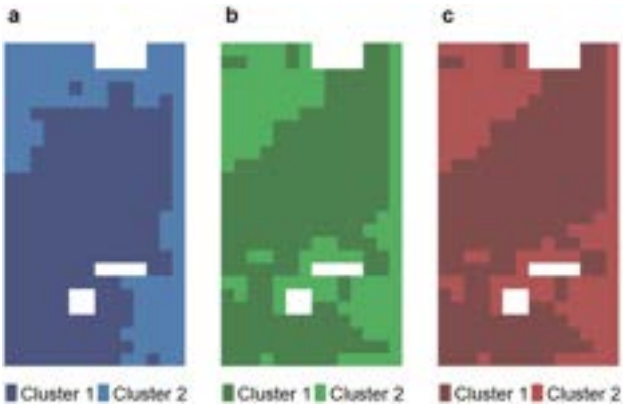

Fig. 3 Time-series clustering maps for satellite-derived **a** evapotranspiration (ET); **b** leaf area index (LAI); and **c** normalized vegetation difference index (NDVI)

Table 1 Average silhouette width (ASW) scores for 2–6 cluster partitioning of evapotranspiration (ET), leaf area index (LAI), and the normalized vegetation difference index (NDVI) time series

Number of clusters	ET	LAI	NDVI
2	**0.41**	**0.49**	**0.47**
3	0.27	0.42	0.44
4	0.24	0.32	0.46
5	0.23	0.27	0.4
6	0.22	0.21	0.39

Values in bold signify the highest ASW value for each dataset, signifying a higher cluster quality

Table 2 Average silhouette width (ASW) values for evaluation of time-series clustering performance for the evapotranspiration (ET), leaf area index (LAI), and normalized difference vegetation index (NDVI) datasets

	ET	LAI	NDVI
Global ASW	0.41	0.49	0.47
Cluster 1 ASW	0.50	0.58	0.58
Cluster 2 ASW	0.25	0.34	0.29

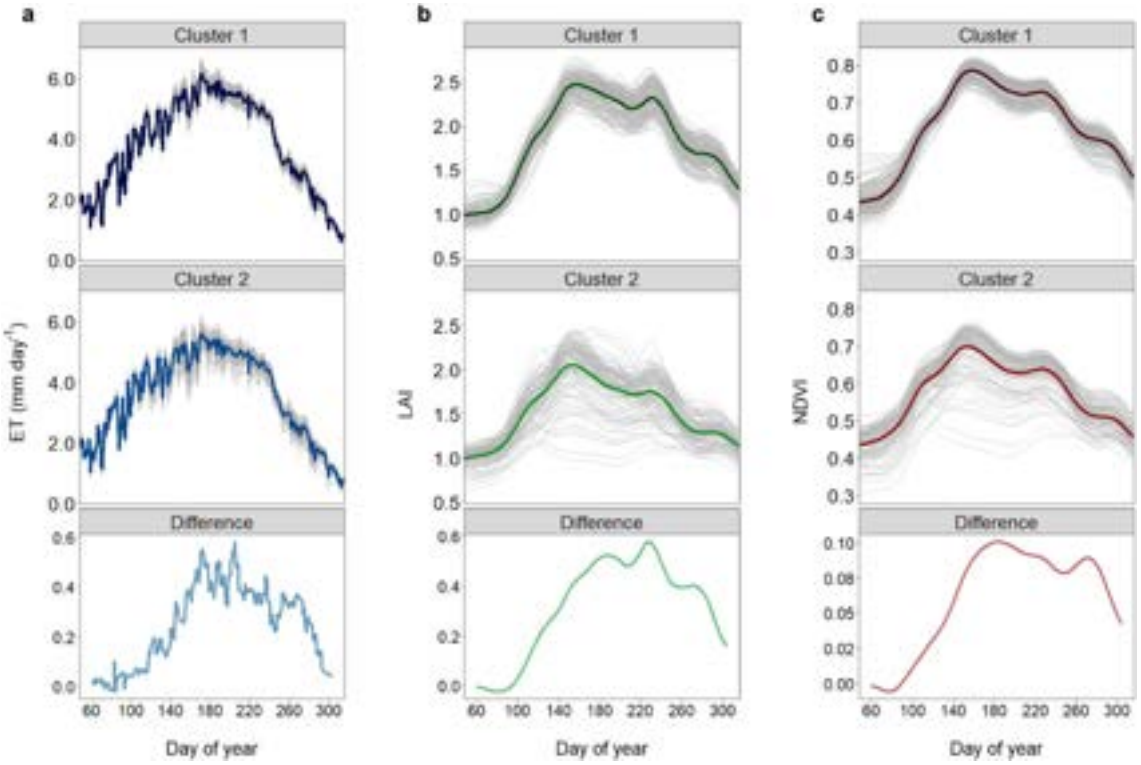

Fig. 4 Time-series clustering plots for satellite retrievals of **a** evapotranspiration (ET, mm day^{-1}); **b** leaf area index (LAI); and normalized vegetation difference index (NDVI). The colored lines are the cluster centers

Table 3 Cluster center difference measures for the evapotranspiration (ET), leaf area index (LAI), and normalized difference vegetation index (NDVI) datasets

	ET (mm day^{-1})	LAI	NDVI
Data range	0.55–6.16	0.99–2.47	0.43–0.79
Cluster centers difference range	− 0.02–0.58	− 0.02–0.58	0–0.1
Difference range normalized to data range	0.11	0.40	0.30

attributed to ET, with the lowest global ASW (Table 2) and lowest difference range to data range ratio (Table 3).

Comparison among ET, LAI, and NDVI time-series clustering

The time-series of cluster centers 1 and 2 for ET, LAI, and NDVI, as well as the difference curves between the cluster centers, were normalized (Fig. 5). The association and similarity statistics (Table 4) show very strong similarities between LAI and NDVI for both the Cramer's V statistic and Fréchet distance for Clusters 1 and 2. ET was found to have a slightly stronger association to LAI than to NDVI. However, for the cluster difference curves, the lowest distance was found between ET and NDVI, signifying higher similarity for the temporal cluster separation dynamic.

Bivariate time-series clustering

An aggregated MZ map for the vineyard was generated using a distance matrix derived from the categorical cluster values (1 and 2) of two datasets. The association between LAI and NDVI was found to be very strong (Table 4), therefore, the LAI TSC map was removed from the analysis. The bivariate clustering was generated using the ET and NDVI TSC maps (Fig. 3) and provided an aggregated MZ map for the vineyard (Fig. 6), with ASW of 0.75. A visualization of a yield map for the 2016 harvest is also provided in Fig. 6b to demonstrate the similarity between the spatial patterns of the bivariate clustering map and yield.

Analysis of the yield map against time-series clustering maps

The results of the statistical tests conducted to assess similarities between the cluster maps spatial patterns and yield spatial distribution are summarized in Table 5. For all datasets, the means of yield were found to be significantly

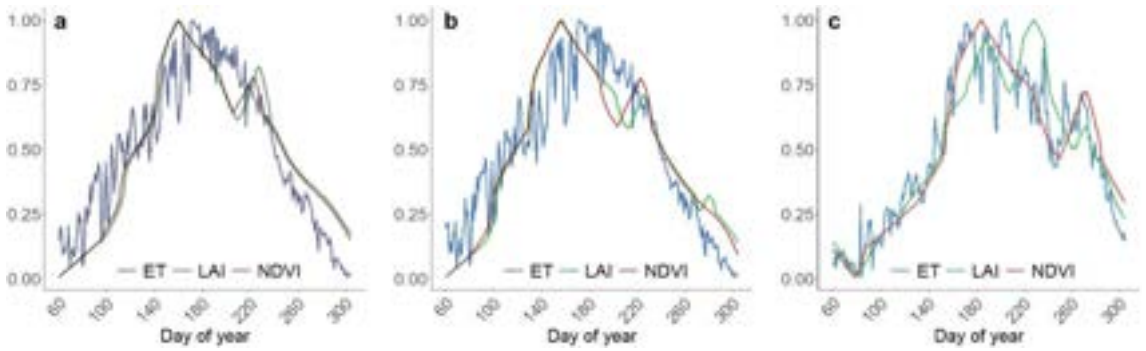

Fig. 5 Normalized values of cluster centers and their differences for **a** normalized values of cluster center 1; **b** normalized values of cluster center 2; and **c** normalized values of cluster centers differences, for evapotranspiration (ET), leaf area index (LAI), and normalized difference vegetation index (NDVI) datasets

Table 4 Cramer's V and Fréchet distance similarity measures of the time series of Cluster center 1, Cluster center 2, and their difference among the evapotranspiration (ET), leaf area index (LAI), and normalized difference vegetation index (NDVI) datasets

	ET-LAI	ET-NDVI	LAI-NDVI
Cramer's V	0.62	0.61	0.97
Fréchet distance cluster center 1	32.89	27.95	4.86
Fréchet distance cluster center 2	29.31	28.83	5.96
Fréchet distance cluster center difference	23.18	17.80	20.37

The Fréchet distance was conducted on the normalized cluster centers

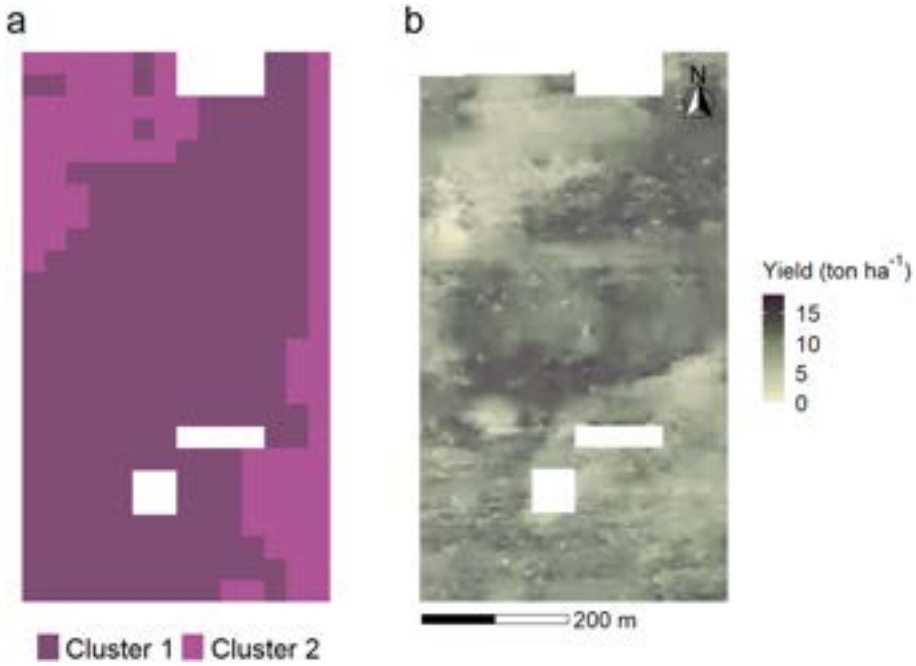

Fig. 6 Bivariate clustering derived from the time-series clustering maps of evapotranspiration (ET) and the normalized difference vegetation index (NDVI) (**a**); and a yield map of the vineyard for the harvest of 2016 (**b**)

different among the two clusters of each map, as well as the distributions of yield values among the two clusters.

Table 5 Differences in yield values among Clusters 1 and 2 of evapotranspiration (ET), leaf area index (LAI), normalized difference vegetation index (NDVI), and the bivariate clustering maps

	ET	LAI	NDVI	Bivariate clustering
Yield mean Cluster 1 (ton ha^{-1})	10.56	10.87	10.90	10.54
Yield mean Cluster 2 (ton ha^{-1})	8.59	8.44	8.44	8.47
t (p value)	4.96 ($p < 0.001$)	7.38 ($p < 0.001$)	7.59 ($p < 0.001$)	4.83 ($p < 0.001$)
D (p value)	0.36 ($p < 0.001$)	0.46 ($p < 0.001$)	0.46 ($p < 0.001$)	0.35 ($p < 0.001$)

Yield means (ton ha^{-1}) for each cluster (e.g., Cluster 1 and Cluster 2) of each map are shown. t test (t) and Kolmogorov–Smirnov (D) statistics determine the differences in means and distribution, respectively, between the yield values in Cluster 1 and Cluster 2 of each map

Discussion

Three sets of time series of satellite-derived images of ET, LAI, and NDVI at a temporal resolution of 1 day were clustered to define MZs in a California vineyard (Fig. 3). The temporal values of each pixel were averaged to represent a seasonal profile and served as input to a FCM clustering algorithm, using two clusters (Table 1). The performance of the clustering algorithm was better for NDVI and LAI (Tables 2, 4), which were shown to have smoother temporal patterns (Fig. 2) than ET. The comparison conducted among the three TSC maps, each clustered into two MZs, showed that NDVI and LAI had a very strong similarity in MZ spatial patterns across the vineyard (Table 4). LAI and NDVI are highly correlated in nature, and many empirical models estimate LAI using the relationship between LAI and NDVI. In this paper, LAI was retrieved using the regression trees trained on LAI-ground measurements and surface reflectance. We included NDVI in this paper since it is a simple index that can be computed from the original surface reflectance directly. ET was found to have a weaker association to LAI and NDVI, both spatially and temporally, while comparing the normalized cluster centers (Fig. 5, Table 4). A final MZ delineation may be conducted using multiple time series to account for various dynamic attributes within the field, as shown in Fig. 6. Finally, the MZs generated for each dataset were shown to be feasible and reliable (Table 5). The analysis of each cluster map determined that the suggested MZs provided a reliable separation of the vineyard into subunits, as significant differences in yield values (2016 harvest) were found among the clusters of each map.

The TSC approach relies on the notion that particular objects (i.e. pixels) have more similar temporal dynamics than do others, thereby enabling the determination of groups having similar temporal patterns (Liao 2005). Consequently, a dissimilarity between cluster centers was observed for each set of data. Table 3 indeed shows that Cluster 1 had higher ASW values for all datasets, with stronger similarities among its assigned observations. However, the degree of differences between the cluster centers of Clusters 1 and 2 for the three datasets was different. The discrepancies among cluster center differences were both in curve structure and the extent of difference between the cluster centers. The cluster center differences for ET, LAI, and NDVI (bottom panels in (Figs. 4, 5c) do not display identical curves and temporal dynamics. Each dataset had different ranges of values and the ratio of the difference range to data range was found to be the highest for LAI (0.4, Table 3), followed by NDVI. This finding supports the higher global ASW values found for LAI followed by NDVI, compared to ET. Furthermore, the values of Fréchet distance among the normalized difference between cluster centers for each dataset (Table 4) show that ET and NDVI were more similar than cluster center differences compared for ET vs. LAI and LAI vs. NDVI. Finally, Table 5 shows that although all MZ maps were found to have significant differences between clusters when analyzing yield values, t and D statistics for LAI and NDVI analyses were higher, signifying stronger differences in yield values and distribution among the two MZs.

The variation in MZ partitioning accuracy and cluster center differences is most likely due to the nature of the datasets. ET was characterized by high fluctuations throughout the growing season caused by changes in atmospheric demand, particularly during the early months of the rainy season, which is exacerbated by variability in cloud cover and is aligned with findings reported by previous studies conducted in vineyards located in Mediterranean regions (Ohana-Levi et al. 2020a,b,c; Vanino et al. 2015). This temporal pattern made ET a more complex dataset to partition while relying on its temporal structure than LAI and NDVI that were both smoothly structured. For future use, ET time series may also be smoothed if achieving stronger cluster partitioning is required. Despite these differences, ET, as well as LAI and NDVI in the Lodi vineyard enabled to effectively utilize the spatial variability in the vineyard based on a 30 m resolution set of images, as previously described in Ohana-Levi et al. (2020a) and Sun et al. (2017). The spatial characteristics of plant conditions in this vineyard are highly correlated to local attributes in the vineyard, such as the soil properties, slope and elevation (Ohana-Levi et al. 2020a).

Seasonal grapevine ET was found to be strongly affected by and associated with canopy structure (Netzer et al. 2009; Williams and Ayars 2005) with a strong temporal autocorrelation (Ohana-Levi et al. 2020a,b,c). ET is also known to be responsive to NDVI levels. For example, Er-Raki et al. (2013) found an exponential relationship between crop coefficient and NDVI ($R^2 = 0.63$) in table grapes in Northwest Mexico. NDVI is also known to be affected by some plant biophysical properties over time, such as the vine water conditions (Geli et al. 2019). These interrelations are apparent in Fig. 5, where the general seasonal cycles of ET, LAI, and NDVI are aligned. The crop conditions are strongly affected by environmental characteristics of the vineyard, such as soil type, elevation, slope, etc. (Ohana-Levi et al. 2020a), affecting all three data types similarly across the field, with some distinctions. Table 4 shows these distinctions between the normalized cluster center curves. LAI and NDVI were found to have very similar temporal patterns, with low Fréchet distance values for cluster centers 1 and 2. Contrarily, ET cluster centers had higher difference levels from LAI and NDVI cluster centers due to the fluctuating structure of the ET data. The strong relations between NDVI and LAI in the vineyard correspond to previous findings in Napa Valley using Ikonos satellite images on multiple grape varieties (Johnson et al. 2003; Johnson 2003). ET was indeed found to have stronger differences in temporal variability than LAI and NDVI. However, the latter two remote-sensing-based canopy measures may still be used for MZs delineation of the vineyard for irrigation applications.

This current work was conducted using a 1 day temporal resolution. However, the proposed analysis may be conducted over various time scales, depending on the scope, extent of available data, and time frame of the study. The user should also consider the temporal autocorrelation of the data. For example, ET was found to have temporal dependence for lags below 5 (Ohana-Levi et al. 2020b), meaning that time intervals of 5 days and above will not fully capture the variations in the seasonal pattern. Temporal clustering can be applied on various scales and temporal resolutions (Granell et al. 2015), however, the analysis should correspond to the predefined objective. The temporal resolution may also affect the decision of the distance measure used in the clustering procedure (Aghabozorgi et al. 2015). In this present study case, ET, LAI, and NDVI were selected as measures of vine conditions, which vary rapidly, especially during critical phenological periods along the growing season (Arab et al. 2021; Knipper et al. 2020; Sun et al. 2017). Therefore, a daily temporal resolution was suitable for the analysis.

This study presented a simple case of TSC, and a comparison among three different datasets. A bivariate clustering approach was also presented (Fig. 6) using categorical maps to generate MZ aggregation. The yield map of the vineyard for the 2016 season shows similar spatial patterns (Table 5), confirming that the MZs generated using the bivariate clustering of ET and NDVI may be accurately applied for SSM purposes. Ohana-Levi et al. (2020a) found a significant relationship between ET TSC for three time-series components and the spatial distribution of yield in the same study site. They reported that the spatial distribution of the MZs was affected by within-field variability in soil type and elevation. Similar relations between MZs and yield for LAI and NDVI (Table 5) suggest that the environmental conditions in the vineyard generate statistically significant variations in the vegetative attributes of the vines, as well as in yield. SSM and TSM may be used to minimize these variations and reach stronger homogeneity across the field during all stages of the growing season. Alternatively, differential harvest may be applied according to theses variations.

The bivariate clustering method suggested in this study may be substituted and applied using various multivariate TSC techniques. For example, the TSC of multiple datasets may be applied by concatenating the multiple variables into a single vector prior to clustering (Wang et al. 2007). A different approach used a principal component analysis (PCA)-based similarity measure between the time series, thus transforming the multivariate time series into a new coordinate space (Li 2019). A feature-based approach suggested converting the raw time-series into a feature vector of lower dimensions, followed by applying a conventional clustering algorithm (Aghabozorgi et al. 2015). The latter approach may facilitate future applications of defining MZs based on multiple time series along with static data in the field (e.g., elevation, lithology, slope, etc.).

MZs based on vegetative attributes and water demand provide valuable information for skilled decision-making and data-driven irrigation applications for existing vineyards, as well as differential harvesting. TSC may also surrogate terrain and soil information from the field for determining spatial patterns, thus eliminating the need for collecting field data. However, not only the spatial variability is represented when using TSC, but also the temporal variability at the pixel scale, the MZ scale, and if required, the vineyard scale. Quantifying the difference in temporal variability among the MZs is useful for field management and irrigation practices during different stages of the growing season. For example, this current study showed that temporal differences among MZs at the beginning and end of the growing seasons were quite small, such that differential irrigation may be effective only during mid-season. Finally, in this era of data deluge and progressive analysis algorithms, there is a growing potential for integrating various types of datasets to extract meaningful information regarding specific processes and minimize uncertainty concerning field management.

Conclusions

In this present study, a technique for generating MZs in agricultural plots using time series of images was proposed. As satellite imagery becomes more abundant, with higher spatial and temporal resolutions, TSC using remote sensing datasets may be further utilized for dealing with spatial variability and heterogeneity in fields for SSM practices. The suggested approach is highly effective when the delineation of the field is conducted based on the seasonal patterns of crop conditions (e.g., water stress, canopy cover, etc.), rather than static field attributes (e.g., soil properties or terrain). The results show that remote sensing retrievals of ET, LAI, and NDVI were suitable choices for partitioning the vineyard into MZs, while higher separability between clusters was found for LAI and NDVI. Using datasets with smoother temporal dynamics may produce a stronger clustering with better separation. Remote-sensing retrievals of NDVI and LAI are much more commonly acquired than ET and may serve as proxies of ET for MZ delineation. However, in cases of limited plant available water or high atmospheric demand (e.g., heat waves), having ET becomes critical in detecting plant stress. Furthermore, multiple datasets may be used to generate an aggregated MZs map, thus basing decision-making processes on more information from the field.

In this study case, images with a spatial resolution of 30 m were used. However, with the new higher resolution sensors, such as Sentinel-2 and VENμS, the suggested approach may also be used in smaller fields and for various timeframes. Moreover, although this manuscript presented a vineyard as a study case, due the high temporal variability and dynamic patterns of grapevines throughout the growing season, the suggested approach may be applied to various crops and different field conditions across diverse climatic regions. Finally, TSC is a valuable method for modeling temporal dynamics over space using remotely sensed data and may be applied to research fields other than agricultural modeling, such as land-cover monitoring, environmental phenomena, meteorological and climatic properties, and more.

Acknowledgements The authors wish to thank the staff of Viticulture, Chemistry and Enology Division of E&J Gallo Winery for logistical support and funding of GRAPEX field and research activities and insight to local irrigation practices. The authors appreciate the cooperation of Mr. Ernie Dosio of Pacific Agri Lands Management, along with the Sierra Loma vineyard staff, providing access to the vineyard and logistical support of GRAPEX field measurement activities. This research was supported in part by the U.S. Department of Agriculture, Agricultural Research Service. Mention of trade names or commercial products in this publication is solely for the purpose of providing specific information and does not imply recommendation or endorsement by the U.S. Department of Agriculture. USDA is an equal opportunity provider and employer.

Author contributions NO-L: conceptualization, software, methods, formal analysis, interpretation, writing, and editing; FG: data collection, conceptualization, methods, software, interpretation, writing, and editing; KK: data collection, conceptualization, methods, software, interpretation, and editing; WPK: conceptualization, data collection, methods, interpretation, and funding acquisition; MCA: data collection and methods; MMA: data collection and interpretation; LAS: data collection; AK: conceptualization, interpretation, writing, and editing.

Funding Funding provided by E. & J. Gallo Winery made possible the acquisition and processing of the vineyard field data and the financial support for the GRAPEX project by a grant from the NASA Applied Sciences–Water Resources Program (Grant Award NNH17AE39I) supported the development of the satellite-based ET product used in this analysis.

Data availability Not applicable.

Code availability Not applicable.

Declarations

Conflict of interest Not applicable.

References

Acevedo-Opazo C, Tisseyre B, Guillaume S, Ojeda H (2008) The potential of high spatial resolution information to define within-vineyard zones related to vine water status. Precision agriculture. Springer, pp 285–302. https://doi.org/10.1007/s11119-008-9073-1

Aghabozorgi S, Wah TY (2014) Effective clustering of time-series data using FCM. Int J Mach Learn Comput 4:170–176. https://doi.org/10.7763/ijmlc.2014.v4.407

Aghabozorgi S, Seyed Shirkhorshidi A, Ying Wah T (2015) Time-series clustering—a decade review. Inf Syst. https://doi.org/10.1016/j.is.2015.04.007

Akoglu H (2018) User's guide to correlation coefficients. Turkish J Emerg Med. https://doi.org/10.1016/j.tjem.2018.08.001

Albornoz EM, Kemerer AC, Galarza R, Mastaglia N, Melchiori R, Martínez CE (2018) Development and evaluation of an automatic software for management zone delineation. Precis Agric 19:463–476. https://doi.org/10.1007/s11119-017-9530-9

Alt H, Godau M (1995) Computing the Frechet distance between two polygonal curves. Int J Comput Geom Appl 05:75–91. https://doi.org/10.1142/s0218195995000064

Anderson MC, Norman JM, Mecikalski JR, Otkin JA, Kustas WP (2007) A climatological study of evapotranspiration and moisture stress across the continental United States based on thermal remote sensing: 1. Model formulation. J Geophys Res Atmos. https://doi.org/10.1029/2006JD007506

Anderson M, Gao F, Knipper K, Hain C, Dulaney W, Baldocchi D, Eichelmann E, Hemes K, Yang Y, Medellin-Azuara J, Kustas W (2018) Field-scale assessment of land and water use change over the California delta using remote sensing. Remote Sens 10:889. https://doi.org/10.3390/rs10060889

Arab ST, Noguchi R, Matsushita S, Ahamed T (2021) Prediction of grape yields from time-series vegetation indices using satellite remote sensing and a machine-learning approach. Remote Sens Appl Soc Environ 22:100485. https://doi.org/10.1016/J.RSASE.2021.100485

Brockwell PJ, Davis RA (2016) Introduction to time series and forecasting, 3rd edn. Springer, Cham

Cammalleri C, Anderson MC, Gao F, Hain CR, Kustas WP (2014) Mapping daily evapotranspiration at field scales over rainfed and irrigated agricultural areas using remote sensing data fusion. Agric for Meteorol 186:1–11. https://doi.org/10.1016/j.agrformet.2013.11.001

Campos I, Neale CMU, Calera A, Balbontín C, González-Piqueras J (2010) Assessing satellite-based basal crop coefficients for irrigated grapes (*Vitis vinifera* L.). Agric Water Manag 98:45–54. https://doi.org/10.1016/j.agwat.2010.07.011

Cebeci Z (2018) Comparison of internal validity indices for fuzzy clustering. Journal of AgriculturalInformatics 10(2):1–14. https://doi.org/10.17700/jai.2019.10.2.537

Claverie M, Ju J, Masek JG, Dungan JL, Vermote EF, Roger JC, Skakun SV, Justice C (2018) The harmonized landsat and sentinel-2 surface reflectance data set. Remote Sens Environ 219:145–161. https://doi.org/10.1016/J.RSE.2018.09.002

Coble KH, Mishra AK, Ferrell S, Griffin T (2018) Big data in agriculture: a challenge for the future. Appl Econ Perspect Policy 40:79–96. https://doi.org/10.1093/aepp/ppx056

Córdoba MA, Bruno CI, Costa JL, Peralta NR, Balzarini MG (2016) Protocol for multivariate homogeneous zone delineation in precision agriculture. Biosyst Eng 143:95–107. https://doi.org/10.1016/J.BIOSYSTEMSENG.2015.12.008

Cunha M, Marçal ARS, Silva L (2010) Very early prediction of wine yield based on satellite data from VEGETATION. Int J Remote Sens 31:3125–3142. https://doi.org/10.1080/01431160903154382

de Azevedo PV, Soares JM, de da Silva VPR, da Silva BB, Nascimento T (2008) Evapotranspiration of "Superior" grapevines under intermittent irrigation. Agric Water Manag 95:301–308. https://doi.org/10.1016/J.AGWAT.2007.10.011

de Jong R, de Bruin S, de Wit A, Schaepman ME, Dent DL (2011) Analysis of monotonic greening and browning trends from global NDVI time-series. Remote Sens Environ 115:692–702. https://doi.org/10.1016/j.rse.2010.10.011

Er-Raki S, Rodriguez JC, Garatuza-Payan J, Watts CJ, Chehbouni A (2013) Determination of crop evapotranspiration of table grapes in a semi-arid region of Northwest Mexico using multi-spectral vegetation index. Agric Water Manag 122:12–19. https://doi.org/10.1016/j.agwat.2013.02.007

Fontanet M, Scudiero E, Skaggs TH, Fernàndez-Garcia D, Ferrer F, Rodrigo G, Bellvert J (2020) Dynamic Management zones for irrigation scheduling. Agric Water Manag 238:106207. https://doi.org/10.1016/j.agwat.2020.106207

Gao F, Masek J, Schwaller M, Hall F (2006) On the blending of the landsat and MODIS surface reflectance: predicting daily landsat surface reflectance. IEEE Trans Geosci Remote Sens 44:2207–2218. https://doi.org/10.1109/TGRS.2006.872081

Gao F, Anderson MC, Kustas WP, Wang Y (2012) Simple method for retrieving leaf area index from Landsat using MODIS leaf area index products as reference. J Appl Remote Sens 6:063554. https://doi.org/10.1117/1.jrs.6.063554

Gao F, Anderson MC, Kustas WP, Houborg R (2014) Retrieving leaf area index from landsat using MODIS LAI products and field measurements. IEEE Geosci Remote Sens Lett 11:773–777. https://doi.org/10.1109/LGRS.2013.2278782

Gao F, Anderson M, Daughtry C, Karnieli A, Hively D, Kustas W (2020) A within-season approach for detecting early growth stages in corn and soybean using high temporal and spatial resolution imagery. Remote Sens Environ 242:111752. https://doi.org/10.1016/j.rse.2020.111752

Gath I, Geva AB (1989) Unsupervised optimal fuzzy clustering. IEEE Trans Pattern Anal Mach Intell 11:773–780. https://doi.org/10.1109/34.192473

Geli HME, González-Piqueras J, Neale CMU, Balbontín C, Campos I, Calera A (2019) Effects of surface heterogeneity due to drip irrigation on scintillometer estimates of sensible, latent heat fluxes and evapotranspiration over vineyards. Water 12:81. https://doi.org/10.3390/w12010081

Gómez C, White JC, Wulder MA (2016) Optical remotely sensed time series data for land cover classification: a review. ISPRS J Photogramm Remote Sens. https://doi.org/10.1016/j.isprsjprs.2016.03.008

Gower JC (1971) A general coefficient of similarity and some of its properties. Biometrics 27:857. https://doi.org/10.2307/2528823

Granell R, Axon CJ, Wallom DCH (2015) Impacts of raw data temporal resolution using selected clustering methods on residential electricity load profiles. IEEE Trans Power Syst 30:3217–3224. https://doi.org/10.1109/TPWRS.2014.2377213

Haghverdi A, Leib BG, Washington-Allen RA, Ayers PD, Buschermohle MJ (2015) Perspectives on delineating management zones for variable rate irrigation. Comput Electron Agric 117:154–167. https://doi.org/10.1016/J.COMPAG.2015.06.019

Hall A, Louis JP, Lamb DW (2008) Low-resolution remotely sensed images of winegrape vineyards map spatial variability in planimetric canopy area instead of leaf area index. Aust J Grape Wine Res 14:9–17. https://doi.org/10.1111/j.1755-0238.2008.00002.x

Johnson LF (2003) Temporal stability of an NDVI-LAI relationship in a Napa Valley vineyard. Aust J Grape Wine Res 9:96–101. https://doi.org/10.1111/j.1755-0238.2003.tb00258.x

Johnson LF, Roczen DE, Youkhana SK, Nemani RR, Bosch DF (2003) Mapping vineyard leaf area with multispectral satellite imagery. Comput Electron Agric 38:33–44. https://doi.org/10.1016/S0168-1699(02)00106-0

Kaufman L, Rousseeuw PJ (1990) Finding groups in data: an introduction to cluster analysis, finding groups in data: an introduction to cluster analysis. Wiley Series in Probability and Statistics. Wiley, Hoboken

Kazmierski M, Glemas P, Rousseau J, Tisseyre B (2011) Temporal stability of within-field patterns of ndvi in non irrigated mediterranean vineyards. J Int Sci Vigne Vin 45:61–73. https://doi.org/10.20870/oeno-one.2011.45.2.1488

Khosla R, Westfall DG, Reich RM, Mahal JS, Gangloff WJ (2010) Spatial variation and site-specific management zones. Geostatistical applications for precision agriculture. Springer Netherlands, Dordrecht, pp 195–219. https://doi.org/10.1007/978-90-481-9133-8_8

Knipper KR, Kustas WP, Anderson MC, Alfieri JG, Prueger JH, Hain CR, Gao F, Yang Y, McKee LG, Nieto H, Hipps LE, Alsina MM, Sanchez L (2019a) Evapotranspiration estimates derived using thermal-based satellite remote sensing and data fusion for irrigation management in California vineyards. Irrig Sci 37:431–449. https://doi.org/10.1007/s00271-018-0591-y

Knipper KR, Kustas WP, Anderson MC, Alsina MM, Hain CR, Alfieri JG, Prueger JH, Gao F, McKee LG, Sanchez LA (2019b) Using high-spatiotemporal thermal satellite ET retrievals for operational water use and stress monitoring in a California vineyard. Remote Sens 11:2124. https://doi.org/10.3390/rs11182124

Knipper KR, Kustas WP, Anderson MC, Nieto H, Alfieri JG, Prueger JH, Hain CR, Gao F, McKee LG, Alsina MM, Sanchez L (2020) Using high-spatiotemporal thermal satellite ET retrievals to monitor water use over California vineyards of different climate, vine variety and trellis design. Agric Water Manag 241:106361. https://doi.org/10.1016/j.agwat.2020.106361

Kumar S, Machiwal D, Dayal D (2017) Spatial modelling of rainfall trends using satellite datasets and geographic information system. Hydrol Sci J 62:1636–1653. https://doi.org/10.1080/02626667.2017.1304643

Kustas WP, Anderson MC, Alfieri JG, Knipper K, Torres-Rua A, Parry CK, Nieto H, Agam N, White WA, Gao F, McKee L, Prueger JH, Hipps LE, Los S, Alsina MM, Sanchez L, Sams B, Dokoozlian N, McKee M, Jones S, Yang Y, Wilson TG, Lei F, McElrone A, Heitman JL, Howard AM, Post K, Melton

F, Hain C (2018) The grape remote sensing atmospheric profile and evapotranspiration experiment. Bull Am Meteorol Soc 99:1791–1812. https://doi.org/10.1175/BAMS-D-16-0244.1
Laurinec P (2018) TSrepr R package: time series representations. J Open Source Softw. https://doi.org/10.21105/joss.00577
Li H (2019) Multivariate time series clustering based on common principal component analysis. Neurocomputing 349:239–247. https://doi.org/10.1016/j.neucom.2019.03.060
Liao WT (2005) Clustering of time series data—a survey. Pattern Recognit 38:1857–1874. https://doi.org/10.1016/j.patcog.2005.01.025
Lilliefors HW (1967) On the Kolmogorov-Smirnov test for normality with mean and variance unknown. J Am Stat Assoc 62:399. https://doi.org/10.2307/2283970
Liu H, Zhan Q, Yang C, Wang J (2018) Characterizing the spatio-temporal pattern of land surface temperature through time series clustering: based on the latent pattern and morphology. Remote Sens 10:654. https://doi.org/10.3390/rs10040654
Maechler M, Rousseeuw PJ, Struyf A, Hubert M, Hornik K (2019) Cluster: cluster analysis basics and extensions. R package version 2.1.0
Maes WH, Steppe K (2012) Estimating evapotranspiration and drought stress with ground-based thermal remote sensing in agriculture: a review. J Exp Bot 63:4671–4712. https://doi.org/10.1093/jxb/ers165
Martínez-Casasnovas JA, Ramos MC, Espinal-Utgés S (2010) Hillslope terracing effects on the spatial variability of plant development as assessed by NDVI in vineyards of the Priorat region (NE Spain). Environ Monit Assess 163:379–396. https://doi.org/10.1007/s10661-009-0842-8
Mathews A, Jensen J (2013) Visualizing and quantifying vineyard canopy LAI using an unmanned aerial vehicle (UAV) collected high density structure from motion point cloud. Remote Sens 5:2164–2183. https://doi.org/10.3390/rs5052164
McBratney A, Whelan B, Ancev T, Bouma J (2005) Future directions of precision agriculture. Precis Agric 6:7–23. https://doi.org/10.1007/s11119-005-0681-8
Militino AF, Moradi M, Ugarte MD (2020) On the performances of trend and change-point detection methods for remote sensing data. Remote Sens 12:1008. https://doi.org/10.3390/rs12061008
Monteith JL, Unsworth MH (2013) Principles of environmental physics plants, animals, and the atmosphere, 4th edn. Elsevier, Oxford
Moritz S, Bartz-Beielstein T (2017) imputeTS: time series missing value imputation in R. R J 9:207–218. https://doi.org/10.32614/RJ-2017-009
Murolo S, Mancini V, Romanazzi G (2014) Spatial and temporal stolbur population structure in a cv. Chardonnay vineyard according to *vmp1* gene characterization. Plant Pathol 63:700–707. https://doi.org/10.1111/ppa.12122
Nawar S, Corstanje R, Halcro G, Mulla D, Mouazen AM (2017) Delineation of soil management zones for variable-rate fertilization: a review. Advances in agronomy. Academic Press Inc, pp 175–245. https://doi.org/10.1016/bs.agron.2017.01.003
Netzer Y, Yao C, Shenker M, Bravdo B-A, Schwartz A (2009) Water use and the development of seasonal crop coefficients for superior seedless grapevines trained to an open-gable trellis system. Irrig Sci. https://doi.org/10.1007/s00271-008-0124-1
Norman JM, Anderson MC, Kustas WP, French AN, Mecikalski J, Torn R, Diak GR, Schmugge TJ, Tanner BCW (2003) Remote sensing of surface energy fluxes at 10 1-m pixel resolutions. Water Resour Res. https://doi.org/10.1029/2002WR001775
Noy K, Ohana-Levi N, Panov N, Silver M, Karnieli A (2021) A long-term spatiotemporal analysis of biocrusts across a diverse arid environment: the case of the Israeli-Egyptian sandfield. Sci Total Environ 774:145154. https://doi.org/10.1016/j.scitotenv.2021.145154
O'Shaughnessy SA, Evett SR, Colaizzi PD (2015) Dynamic prescription maps for site-specific variable rate irrigation of cotton. Agric Water Manag 159:123–138. https://doi.org/10.1016/J.AGWAT.2015.06.001
Ohana-Levi N, Bahat I, Peeters A, Shtein A, Netzer Y, Cohen Y, Ben-Gal A (2019a) A weighted multivariate spatial clustering model to determine irrigation management zones. Comput Electron Agric 162:719–731. https://doi.org/10.1016/J.COMPAG.2019.05.012
Ohana-Levi N, Paz-Kagan T, Panov N, Peeters A, Tsoar A, Karnieli A (2019b) Time series analysis of vegetation-cover response to environmental factors and residential development in a dryland region. Gisci Remote Sens. https://doi.org/10.1080/15481603.2018.1519093
Ohana-Levi N, Knipper KR, Kustas WP, Anderson MC, Netzer Y, Gao F, Alsina MM, Sanchez LA, Karnieli A (2020a) Using satellite thermal-based evapotranspiration time series for defining management zones and spatial association to local attributes in a vineyard. Remote Sens. https://doi.org/10.3390/rs12152436
Ohana-Levi N, Munitz S, Ben-Gal A, Netzer Y (2020b) Evaluation of within-season grapevine evapotranspiration patterns and drivers using generalized additive models. Agric Water Manag 228:105808. https://doi.org/10.1016/j.agwat.2019.105808
Ohana-Levi N, Munitz S, Ben-Gal A, Schwartz A, Peeters A, Netzer Y (2020c) Multiseasonal grapevine water consumption—drivers and forecasting. Agric for Meteorol 280:107796. https://doi.org/10.1016/J.AGRFORMET.2019.107796
Ohana-Levi N, Ben-Gal A, Peeters A, Termin D, Linker R, Baram S, Raveh E, Paz-Kagan T (2021) A comparison between spatial clustering models for determining N-fertilization management zones in orchards. Precis Agric. https://doi.org/10.1007/s11119-020-09731-5
Park YL, Krell RK, Carroll M (2007) Theory, technology, and practice of site-specific insect pest management. J Asia Pac Entomol 10:89–101. https://doi.org/10.1016/S1226-8615(08)60337-4
Pathak HS, Brown P, Best T (2019) A systematic literature review of the factors affecting the precision agriculture adoption process. Precis Agric. https://doi.org/10.1007/s11119-019-09653-x
Peralta NR, Costa JL, Balzarini M, Castro Franco M, Córdoba M, Bullock D (2015) Delineation of management zones to improve nitrogen management of wheat. Comput Electron Agric 110:103–113. https://doi.org/10.1016/J.COMPAG.2014.10.017
Petitjean F, Inglada J, Gançarski P (2012) Satellite image time series analysis under time warping. IEEE Trans Geosci Remote Sens 50:3081–3095. https://doi.org/10.1109/TGRS.2011.2179050
R Core Team (2020) R: a language and environment for statistical computing. R Foundation for StatisticalComputing, Vienna, Austria. https://www.R-project.org/
Reynolds AP, Richards G, De La Iglesia B, Rayward-Smith VJ (2006) Clustering rules: a comparison of partitioning and hierarchical clustering algorithms. J Math Model Algorithms 5:475–504. https://doi.org/10.1007/s10852-005-9022-1
Romani LAS, Gonçalves RRV, Amaral BF, Chino DYT, Zullo J, Traina C, Sousa EPM, Traina AJM (2011) Clustering analysis applied to NDVI/NOAA multitemporal images to improve the monitoring process of sugarcane crops, in: 2011 6th International Workshop on the Analysis of Multi-Temporal Remote Sensing Images, Multi-Temp 2011—Proceedings. pp. 33–36. https://doi.org/10.1109/Multi-Temp.2011.6005040
Rousseeuw PJ (1987) Silhouettes: a graphical aid to the interpretation and validation of cluster analysis. J Comput Appl Math 20:53–65. https://doi.org/10.1016/0377-0427(87)90125-7
Semmens KA, Anderson MC, Kustas WP, Gao F, Alfieri JG, McKee L, Prueger JH, Hain CR, Cammalleri C, Yang Y, Xia T, Sanchez L, Mar Alsina M, Vélez M (2016) Monitoring daily evapotranspiration over two California vineyards using Landsat 8

in a multi-sensor data fusion approach. Remote Sens Environ 185:155–170. https://doi.org/10.1016/j.rse.2015.10.025

Sun L, Gao F, Anderson M, Kustas W, Alsina M, Sanchez L, Sams B, McKee L, Dulaney W, White W, Alfieri J, Prueger J, Melton F, Post K (2017) Daily mapping of 30 m LAI and NDVI for grape yield prediction in California vineyards. Remote Sens 9:317. https://doi.org/10.3390/rs9040317

Tucker CJ (1979) Red and photographic infrared linear combinations for monitoring vegetation. Remote Sens Environ 8:127–150. https://doi.org/10.1016/0034-4257(79)90013-0

Vanino S, Pulighe G, Nino P, De Michele C, Bolognesi S, D'Urso G (2015) Estimation of evapotranspiration and crop coefficients of tendone vineyards using multi-sensor remote sensing data in a mediterranean environment. Remote Sens 7:14708–14730. https://doi.org/10.3390/rs71114708

Viovy N (2000) Automatic classification of time series (acts): a new clustering method for remote sensing time series. Int J Remote Sens 21:1537–1560. https://doi.org/10.1080/014311600210308

Wang X, Wirth A, Wang L (2007) Structure-based statistical features and multivariate time series clustering, In: Proceedings—IEEE International Conference on Data Mining, ICDM. pp. 351–360. https://doi.org/10.1109/ICDM.2007.103

Watson DJ (1947) Comparative physiological studies on the growth of field crops: I. variation in net assimilation rate and leaf area between species and varieties, and within and between years. Ann Bot 11:41–76. https://doi.org/10.1093/oxfordjournals.aob.a083148

Whelan BM, Mcbratney AB, Minasny B (2002) Vesper 1.5-spatial prediction software for precision agriculture, In: Rust R, Larson W (Eds), Precision Agriculture, Proceedings of the 6th International Conference of Precision Agriculture, Madison, Wisconsin. ASA/CSSA/ SSSA, Madison, Wisconsin

White WA, Alsina MM, Nieto H, McKee LG, Gao F, Kustas WP (2018) Determining a robust indirect measurement of leaf area index in California vineyards for validating remote sensing-based retrievals. Irrig Sci 37:269–280. https://doi.org/10.1007/s00271-018-0614-8

Williams LE, Ayars JE (2005) Water use of Thompson Seedless grapevines as affected by the application of gibberellic acid (GA3) and trunk girdling—practices to increase berry size. Agric for Meteorol 129:85–94. https://doi.org/10.1016/j.agrformet.2004.11.007

Xia T, Kustas WP, Anderson MC, Alfieri JG, Gao F, McKee L, Prueger JH, Geli HME, Neale CMU, Sanchez L, Alsina MM, Wang Z (2016) Mapping evapotranspiration with high-resolution aircraft imagery over vineyards using one- and two-source modeling schemes. Hydrol Earth Syst Sci 20:1523–1545. https://doi.org/10.5194/hess-20-1523-2016

Xu L, Zhang H, Wang C, Zhang B, Liu M (2018) Crop classification based on temporal information using sentinel-1 SAR time-series data. Remote Sens 11:53. https://doi.org/10.3390/rs11010053

Zhang N, Wang M, Wang N (2002) Precision agriculture—a worldwide overview. Comput Electron Agric 36:113–132. https://doi.org/10.1016/S0168-1699(02)00096-0

Zhang Z, Tang P, Huo L, Zhou Z (2014) MODIS NDVI time series clustering under dynamic time warping. Int J Wavelets Multiresolut Inf Process. https://doi.org/10.1142/s0219691314610116

Zhang L, Weng Q, Shao Z (2017) An evaluation of monthly impervious surface dynamics by fusing Landsat and MODIS time series in the Pearl River Delta, China, from 2000 to 2015. Remote Sens Environ 201:99–114. https://doi.org/10.1016/j.rse.2017.08.036